ACS Catalysis

Research Article

Cite This: ACS Catal. 2019, 9, 7578–7587

pubs.acs.org/acscatalysis

Electro-Oxidation of Methane on Platinum under Ambient Conditions

Michael J. Boyd,[†,‡] Allegra A. Latimer,[†,‡] Colin F. Dickens,[†,‡] Adam C. Nielander,[†,‡] Christopher Hahn,[†,‡] Jens K. Nørskov,[*,∥] Drew C. Higgins,[*,†,‡,§] and Thomas F. Jaramillo[*,†,‡]

[†]Department of Chemical Engineering, Stanford University, Stanford, California 94305, United States

[‡]SUNCAT Center for Interface Science and Catalysis, SLAC National Accelerator Laboratory, Menlo Park, California 94025, United States

[§]Department of Chemical Engineering, McMaster University, Hamilton, ON, Canada L8S 4L7

[∥]Surface Physics and Catalysis, Department of Physics, Technical University of Denmark, 2800 Kgs. Lyngby, Denmark

Supporting Information

ABSTRACT: Herein, we investigate the electrochemical conversion of methane to CO_2 on platinum electrodes under ambient conditions. Through a combination of experimentation, density functional theory (DFT) calculations, and ab initio kinetic modeling, we have developed an improved understanding of the reaction mechanism and the factors that determine catalyst activity. We hypothesized that the rate-determining methane activation step is thermochemical (i.e., $CH_4(g) \rightarrow CH_3^* + H^*$) as opposed to electrochemical based on a fitted barrier of approximately 0.96 eV that possesses minimal potential dependence. We developed a simple kinetic model based on the assumption of thermochemical methane activation as the rate-determining step, and the results match well with experimental data. Namely, the magnitude of the maximum current density and the electrode potential at which it is realized agree with our ab initio kinetic model. Finally, we expanded our kinetic model to include other transition metals via a descriptor-based analysis and found platinum to be the most active catalyst for the oxidation of methane, which is in line with previously published experimental observations.

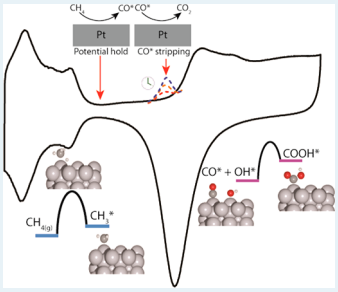

KEYWORDS: *platinum, methane, electro-oxidation, DFT, kinetic modeling*

1. INTRODUCTION

Methane is the primary component of natural gas, a worldwide energy resource that has seen a rapid growth in global production because of the development of shale gas resources. However, a major technical challenge in natural gas utilization is transportation. As a result of the high costs associated with the transport of natural gas, approximately 200 billion cubic feet are flared annually in the United States alone.[1] Although flaring mitigates the direct release of natural gas, a potent greenhouse gas, it accounts for the annual emission of ∼12.7 million tonnes of CO_2. Thus, there are clear economic and environmental incentives to develop low-cost, distributed technologies that can directly convert methane and other natural gas components (e.g., ethane, propane) into value added products. Ideas for such technologies include the chemical transformation of methane into more valuable, higher-boiling-point chemicals (e.g., methanol) and electrochemical processes to convert methane to electricity under near-ambient conditions.

The selective partial oxidation of methane is a challenging endeavor, as the activation energy required to initiate methane oxidation is high, and the resulting reaction intermediates are both more reactive than methane and significantly less stable than the final oxidation product, CO_2.[2] Thus, once oxidation begins, it is difficult to prevent methane from fully oxidizing to CO_2, representing no improvement over the flaring process unless methane is converted electrochemically to yield electricity. Despite these challenges, the partial oxidation of methane to methanol has been extensively explored in the fields of both homogeneous[3,4] and heterogeneous catalysis.[5−13] An alternative to these processes is the electrochemical oxidation of methane. Solid oxide fuel cells (SOFCs) are the most studied devices for this application and are commercially available.[14] Commercial SOFCs require high temperatures (>700 °C) for operation and, as such, offer fast kinetics for the complete oxidation of methane to CO_2,[15] suitable for producing electricity. There are challenges, however, with the operating temperature and pressure of SOFCs, including the need for additional infrastructure and long start-up/shutdown times, which may mitigate their use in remote locations and/or for "on-demand" applications. A less explored option that is better-suited for distributed methane utilization (and perhaps selective oxidation) is the oxidation of methane in low-temperature (<100 °C) electrochemical devices. Electrochemical devices such as polymer electrolyte fuel cells (PEFCs) operate at ∼80 °C and near-ambient pressure. The

Received: March 23, 2019
Revised: June 14, 2019
Published: July 25, 2019

DOI: 10.1021/acscatal.9b01207
ACS Catal. 2019, 9, 7578–7587

relevant electrochemical half-reactions for methane conversion can be seen in eqs 1 and 2 below.

$$CH_4 + 2H_2O \rightleftharpoons CO_2 + 8H^+ + 8e^- \quad E_{rev} = 0.17\ V\ vs.\ RHE \tag{1}$$

$$CH_4 + H_2O \rightleftharpoons CH_3OH + 2H^+ + 2e^- \quad E_{rev} = 0.65\ V\ vs.\ RHE \tag{2}$$

In these devices, the electrode potential is used to tune the reaction thermodynamics and kinetics, analogous to the way temperature and pressure steer thermal catalytic processes. Because of the near-ambient operating conditions of electrochemical devices, low-temperature PEFCs are a decentralized technology and could be implemented at the well head so that methane could be directly converted electrochemically into more easily transported chemicals such as methanol (while producing electricity) or fully oxidized to CO_2 to generate electricity.

Early investigations into hydrocarbon PEFCs were conducted using platinum black anodes. The performance of PEFCs running on methane, ethylene, propane, carbon monoxide, and hydrogen were studied.[16,17] It was observed that PEFC performance when using hydrocarbons was significantly worse than when using carbon monoxide or hydrogen, likely because of the difficulty of breaking C−H and C−C bonds at typical operating temperatures (<100 °C). The PEFC performance was the lowest in the case of methane, which is known to have the least reactive C−H bonds of these alkanes.[2] To gain mechanistic insight into the activation and adsorption processes for methane and other hydrocarbons on platinum electrodes, the system was studied under "potentiodynamic" conditions, in which the electrode potential was first held for an extended period of time to activate methane, followed by linear sweep voltammetry to more positive electrode potentials to strip adsorbed intermediates from the catalyst surface.[18−23] It was found that during the electrode potential hold, methane is activated and forms C1 species on the electrode surface, which may be partially oxygenated. However, specific speculation into the reaction mechanism could not be performed on the basis of electrochemical experiments alone. In situ IR spectroscopy was later performed using external reflection in an attempt to observe intermediate species.[24] The authors observe CO/CHO intermediates on platinum as well as the final product CO_2. Further insight into the reaction mechanism for methane oxidation on the surface of platinum electrodes can provide guidance for the development of new catalysts and alternate reaction schemes.

In this work, we present a joint experimental and computational study of the complete electrochemical oxidation of methane on platinum electrodes. Electrochemical experiments were performed to determine methane oxidation activity as a function of electrode potential and time, and the optimum electrode potential for continuous methane oxidation was determined. We hypothesize that the methane activation step is thermochemical (i.e., $CH_4(g) \rightarrow CH_3^* + H^*$) as opposed to electrochemical based on a fitted barrier of approximately 0.96 eV that possesses minimal potential dependence. We employed density functional theory (DFT) calculations and kinetic modeling to aid in the interpretation of the experimental observations and to provide insight into the reaction pathway. Leveraging this mechanistic understanding of electrochemical methane oxidation on Pt, we extend our computational analysis to include other transition metal catalysts and discuss why platinum has been the best catalyst demonstrated for methane electro-oxidation to date. The combination of experiment and theory presented herein provides a fundamental understanding of low-temperature electrochemical methane oxidation and offers guidance for the design of future methane oxidation catalysts.

2. METHODS

2.1. Electrode Preparation. Platinum foils (Alfa Aesar, 99.95% metals basis) were used for both the working and counter electrodes. Platinum electrodes were flame annealed with a butane torch prior to use. The working electrode was platinized via electrodeposition using a solution containing 10 mM H_2PtCl_6 (99.995% metals basis, Sigma-Aldrich) in 0.5 M $HClO_4$ (GFS Chemicals, Veritas double distilled). The platinization procedure consisted of a pulse electrodeposition, in which the platinum working electrode was cycled between a galvanostatic hold at −10 mA cm^{-2} and open circuit potential (OCP) (1 s reduction followed by 6 s at OCP) for 100 cycles to generate a high-surface-area electrode. X-ray photoelectron spectroscopy (XPS, PHI Versaprobe) and scanning electron microscopy (SEM, FEI XL30 Sirion) were used to characterize the surface of the electrode after electrodeposition.

2.2. Methane Adsorption Experiments. All containers, glassware, and reaction vessels were thoroughly cleaned by soaking in piranha solution (3:1, sulfuric acid/30% H_2O_2) for 24 h to remove trace organics and impurities that could convolute the electrochemical oxidation features observed after methane adsorption. After soaking in piranha solution, the containers and contents were rinsed several times with Millipore water (18.2 MΩ cm) and stored in Millipore water to prevent contamination.

A custom electrochemical cell, shown in SI section 1, Figure S1, and modified from a design described previously,[25] made of Kel-F and fitted with FEP encapsulated silicone o-rings (McMaster-Carr) was utilized for all methane oxidation experiments. A Nafion membrane was used to separate the working electrode and counter electrode compartments for the long-term chronoamperometry experiments; otherwise, no membrane was used. The platinum working and counter electrodes have an exposed area of 6 cm^2, and the total electrolyte volume was 20 mL with 10 mL of headspace. The reference electrode (Ag/AgCl, Accumet) was connected to the electrochemical cell via a fritted Luggin capillary. The reference electrode was calibrated prior to electrochemical tests using a reversible hydrogen electrode (RHE) standard. Electrochemical measurements were performed using a Bio-Logic VMP3 potentiostat and performed inside of a custom Faraday cage to reduce experimental noise. During measurements, the potentiostat compensated for 85% of the electrolyte resistance, and the last 15% was accounted for during data analysis to arrive at the true working electrode potential. The platinum working electrode was electrochemically cleaned in a Ar-sparged 0.5 M $HClO_4$ solution by sweeping the electrode potential between 0 and 1.6 V vs RHE at 200 mV/s for 100 cycles or until a stable cyclic voltammogram (CV) was achieved. Electrochemically active surface areas (ECSAs) reported throughout this work were determined by conducting CVs at a scan rates of 50 mV/s and integrating the charge transferred in the hydrogen underpotential deposition (H_{UPD}) region (see SI section 2, Figure S2). A value of 210 mC cm^{-2} was used to correlate charge transfer to ECSA. The electrochemical cell was sparged with either argon (Research

DOI: 10.1021/acscatal.9b01207
ACS Catal. 2019, 9, 7578−7587

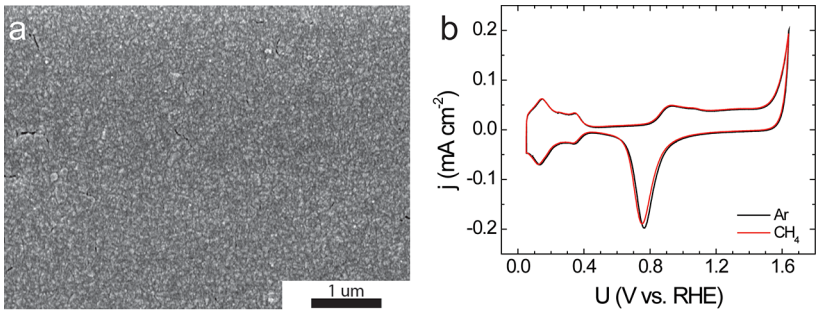

Figure 1. Characterization of platinized platinum electrode. (a) SEM image of electrode surface after electrochemical testing. (b) Representative CV (50 mV/s) of high-surface-area platinum electrodes (~240 cm^2 ECSA) in 0.5 M perchloric acid with Ar (black) and CH_4 (red) purge.

grade 5.0, Praxair) or methane (Research grade 5.0, Praxair) for 30 min to equilibrate the electrolyte and headspace, after which the cell was sealed. The methane was fed through a Matheson NANOCHEM purifier for the removal of CO and nonmethane hydrocarbons. Electrochemical experiments performed under argon were used as a control and baseline for determining methane oxidation activity as a function of electrode hold potential (U_{hold}) and time (t_{hold}). The electrochemical measurements were designed based on previous work.[18] Briefly, the electrode potential was held constant between 0.2 and 0.6 V vs RHE in order to activate methane, followed by a stripping phase where the electrode potential was swept at 50 mV/s to 1.4 V vs RHE to oxidize adsorbed intermediates from the surface. For chronoamperometry and cyclic voltammetry, the charge transfer observed under argon saturated electrolyte was subtracted from that observed under methane saturated electrolyte to determine the activity.

2.3. DFT Calculations. The plane-wave QuantumEspresso code[26] and RPBE[27] functional were used for the density functional theory (DFT)[28,29] calculations. The plane-wave and density energy cutoffs were 600 and 6000 eV, respectively. Forces on all atoms were minimized to 0.05 eV $Å^{-1}$. The (211) stepped surface was chosen as a model for the active site on platinum. A (3,3,1) k-point sampling was employed on 3 × 3 or 3 × 4 supercells of fcc(211) or hcp(10$\bar{1}$0) metals, respectively. Metal slabs were composed of four layers separated by 16 Å vacuum; the lowest two layers were kept fixed to simulate the bulk. Dipole corrections were used for all surface calculations. Climbing-image nudged elastic band (CI-NEB)[30,31] calculations were used to find transition states (TS). Ultrasoft pseudopotentials from the GBRV library were used.[32] Adsorption free energies were referenced to gaseous H_2O at its room temperature vapor pressure (i.e., liquid H_2O) and gas-phase CH_4 and H_2 at 1 bar and were calculated using the harmonic adsorbate approximation for adsorbates and the ideal gas limit for gases.[33] It has previously been noted[34,35] that the RPBE description of certain gas-phase formation energies are inconsistent with experimental values. In particular, the water−gas shift reaction is known to be one such case and is of critical importance in studying methane oxidation chemistry. It was found that the majority of the error is associated with the OCO backbone; in this study, we assume the DFT error lies solely on CO_2(g) and correct its energy to achieve the correct experimental equilibrium potential for the overall reaction (0.17 V). We chose the CO_2 pressure in our kinetic model to be 0.001 atm, approximately the average ambient indoor level.

3. RESULTS AND DISCUSSION

3.1. Preparation and Characterization of Platinized Platinum Electrodes. The high-symmetry and nonpolar nature of the methane molecule render significant molecular activation under ambient temperatures and pressures challenging. Therefore, to increase the amount of platinum catalyst surface area available to catalyze the reaction, platinum foils were platinized in a 0.5 M $HClO_4$ electrolyte containing chloroplatinic acid. This platinization process generates higher-surface-area electrodes, which possess lower surface atom coordination numbers on average and thus higher reactivity.[36] A SEM image of the platinum electrode surface after platinization followed by an electrochemical cleaning procedure consisting of 100 CV cycles from 0.05 to 1.6 V vs RHE at 200 mV/s is shown in Figure 1a. Electrochemical cycling was necessary to produce a stable (i.e., consistent between experiments) surface for consecutive experiments. After electrochemical cycling, there was significant smoothing of the electrode surface as the ECSA dropped from ~450 to ~200 cm^2, corresponding to roughness factors (RFs) of ~75 and ~30. It is also important that, following this procedure, the electrochemical cell and electrodes remain free of contaminants so that any electrochemical signals observed can be attributed to the activity of platinum for methane activation. XPS was used to assess the purity of the electrode surface (post platinization) both before and after electrochemical cycling (see SI section 3, Figure S4) as described in section 2.2. Before electrochemical cycling, chlorine is present in the XPS spectrum along with platinum, oxygen, and carbon. After electrochemical cycling, no chlorine signal is observed, within the detection limits of XPS, indicating that the catalyst surface is clean of significant chlorine or metal impurities.

Figure 1b displays representative CV data for the cleaned platinized platinum electrodes under both methane (reactive) and argon (inert) atmosphere. No significant differences in redox features were observed between voltammograms obtained under argon or methane. Notably, the complete electrochemical oxidation of methane to CO_2 is thermodynamically feasible at electrode potentials positive of 0.17 V vs RHE (eq 1), and the lack of any detectable differences between the current−voltage behavior in either inert or reactive atmosphere may be attributed to significant kinetic barriers for methane activation.[37] The CV behavior observed in Figure 1b is consistent with the standard behavior of platinum, including H_{UPD}, from ~0.05−0.40 V vs RHE, and hydroxide adsorption and/or PtO_x formation, from ~0.80−1.40 V vs RHE. As these adsorption processes are likely kinetically facile in comparison to methane activation, the majority of

DOI: 10.1021/acscatal.9b01207
ACS Catal. 2019, 9, 7578−7587

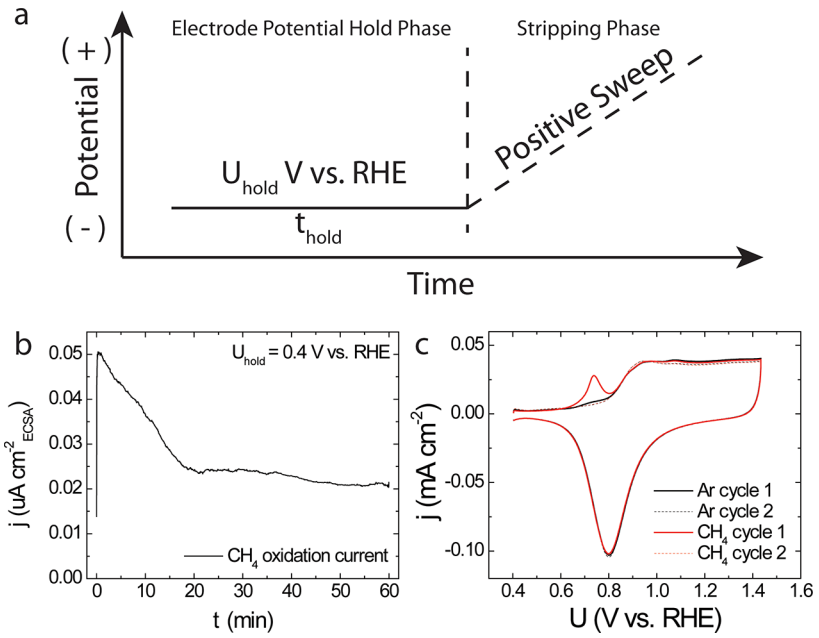

Figure 2. Electrochemical experiments for methane adsorption. (a) Diagram outlining the electrode potential sequences applied to activate methane and oxidize methane-derived intermediates from the electrode surface. (b) Argon background subtracted chronoamperometry during the methane activation phase in 0.5 M perchlroic acid at an applied electrode potential of 0.4 V vs RHE. (c) Cyclic voltammetry showing the oxidation feature after the electrode potential hold when purging with methane (red) compared to the inert argon purge (black). (ECSA ~235 cm^2, scan rate 50 mV/s).

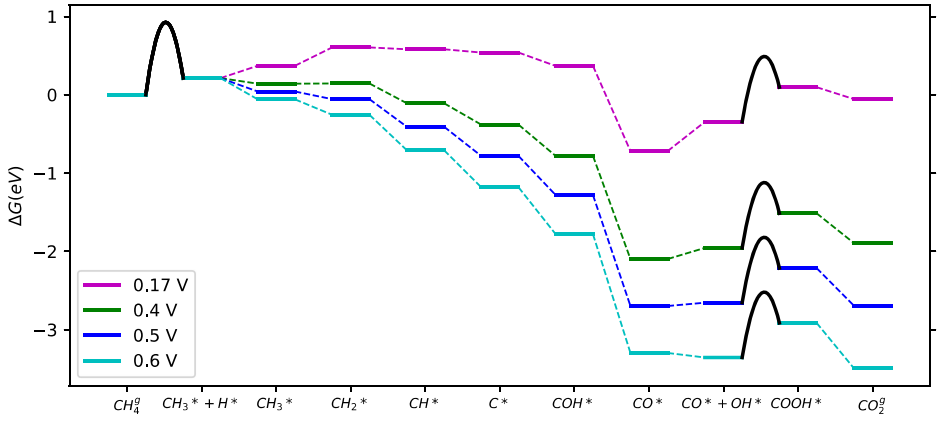

Figure 3. Free energy diagram at 300 K and 1 bar gas-phase pressures for the complete electrochemical oxidation of methane to carbon dioxide on Pt(211) at four representative electrode potentials: 0.17 (the equilibrium potential), 0.40, 0.50, and 0.60 V vs RHE. The *x*-axis labels denote the relevant surface species for each step.

catalytically active sites will likely be occupied by either hydrogen or hydroxide/oxygen in the associated electrode potential regions. Therefore, methane activation is most likely to occur in the electrode potential region between 0.40 and 0.80 V vs RHE, where the surface is free of any strongly bound adsorbates. We note the recently proposed hypothesis that such an adsorbate-free region does not exist at the Pt steps[38−41] (as OH* directly displaces H*); this point will be revisited when we analyze our results.

3.2. Methane Activation via Potential Control. To facilitate the activation of methane and build up a coverage of methane oxidation intermediates on the surface of platinum, the electrode potential was held constant for 1 h at different electrode potentials in the range of 0.2−0.6 V vs RHE. Following this, any adsorbed species were electrochemically stripped from the electrode surface by CV sweeps to more positive electrode potentials,[18] as depicted in Figure 2a. The activity of the platinum electrode for methane activation at a specific electrode hold potential and hold time was assessed by comparing the chronoamperometric (CA) and CV data obtained under the reactive methane atmosphere to that collected under an inert argon atmosphere. The total activity for methane oxidation was assessed by integrating the CA and CV data in the electrode potential hold and stripping phases in methane saturated electrolyte, respectively, and subtracting the values obtained in argon saturated electrolyte as a background.

Figure 2b shows the argon background subtracted current density as a function of time during the electrode potential hold for methane oxidation at 0.4 V vs RHE. After the electrode potential hold, the CV sweep to a more positive electrode potential is shown in Figure 2c. The oxidation feature centered at 0.75 V vs RHE during cycle 1 in Figure 2c

DOI: 10.1021/acscatal.9b01207
ACS Catal. 2019, 9, 7578−7587

is consistent with those observed in previous studies of electrochemical methane oxidation[18] and is also in a similar region to oxidation features observed during CO-stripping experiments on platinum.[42] Cycle 2 in Figure 2c immediately follows cycle 1, and no oxidation feature is observed, allowing us to conclude that all methane intermediate species are oxidized in the first cycle, and insignificant quantities of methane are activated in the second cycle.

To ensure that this oxidative feature is not due to the presence of CO contaminants in the methane feed, the amount of stripping charge that would be observed by oxidizing all contaminant CO in the electrolyte and headspace was calculated. The calculated charge was negligible compared to the oxidation feature observed in Figure 2c, indicating that potential CO contaminants in the methane feed gas do not affect our results (see Table S2 and SI section 5 for more details).

Given the electrode potential where the stripping feature is observed in the context of similar previous experimental observations,[42−44] we believe the methane-derived intermediate is likely CO*. To further explore this hypothesis, we calculated the free energy diagram for complete electrochemical methane oxidation using DFT. We modeled the reaction on undercoordinated sites, because (a) the catalyst employed in this study possesses a high roughness factor, and (b) methane activation barriers on terraces are known to be too high to observe considerable methane oxidation at 300 K.[37] The (211) stepped surface was chosen as a model for undercoordinated sites as is commonly described in the literature.[45,46] A number of reaction intermediates were considered (see SI section 4, Figure S5 for details), and the lowest energy pathway is displayed at four different electrochemical potentials in Figure 3. The release of a single proton−electron pair is implied between each reaction step, except for the two thermochemical steps considered ($CH_4(g) \rightarrow CH_3^* + H^*$ and $CO^* + OH^* \rightarrow COOH^*$). In steps where oxygen is added to the surface (i.e., $C^* \rightarrow COH^*$ and $CO^* \rightarrow CO^* + OH^*$), the consumption of a water molecule is implied.

In this study, we have only calculated barriers for methane activation ($CH_4(g) \rightarrow CH_3^* + H^*$) and CO−OH coupling ($CO^* + OH^* \rightarrow COOH^*$), which we are treating as thermal (nonelectrochemical) steps. This is indicated in Figure 3, where explicitly calculated thermal barriers are shown as black solid curves, and electrochemical steps in which no barriers have been explicitly calculated are shown as dashed lines. We do not calculate electrochemical barriers, as this would require an explicit consideration of the water structure at the surface and modeling of the electrochemical interface, which is computationally challenging and outside the scope of this study. Furthermore, because methane activation is often found to be rate-determining,[2,47−50] we do not expect our neglect of the electrochemical barriers to be problematic. Kinetics will be discussed in further detail in Section 3.4. From this diagram, we can see that CO* is the lowest energy surface species at the potentials considered. If all electrochemical barriers between intermediates are indeed small relative to the barrier associated with methane activation ($CH_4(g) \rightarrow CH_3^* + H^*$), then this picture further supports the hypothesis that the methane-derived intermediate being oxidized in the stripping phase is CO*.

3.3. Methane Oxidation as a Function of Electrode Hold Potential. The effect of the electrode potential was investigated, with Figure 4a showing the electrochemical-

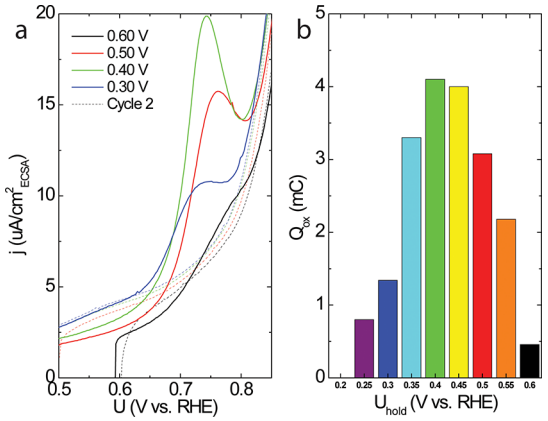

Figure 4. (a) Electrode potential dependence of oxidation feature in 0.5 M perchloric acid after holding the electrode potential constant for 30 min (ECSA ~220 cm^2, scan rate 50 mV/s). (b) Total integrated stripping charge for the different electrode hold potentials.

stripping features demonstrated after the electrode potential hold step was performed at several potentials. The total stripping charge, after activating methane for 30 min at electrode hold potentials ranging from 0.2 to 0.6 V vs RHE in increments of 50 mV, is shown in Figure 4b (see SI section 6, Figures S6−S8 for all CVs). On the basis of these results, the optimum electrode hold potential for building up the highest coverage of CO* intermediates on the surface of platinum after 30 min is 0.4 V vs RHE. Although this optimum electrode hold potential is slightly higher than those reported previously (0.3 and 0.26 V vs RHE), these studies cannot be directly compared, as they differ with respect to catalyst morphology, electrolyte, and operating temperature (65 and 60 °C) (refs 18, 23, respectively).

At electrode hold potentials more negative than 0.4 V vs RHE (i.e., within the H_{UPD} region), we expect adsorbed hydrogen to cover a significant fraction of the platinum surface. If these adsorbed hydrogen atoms are competing with methane adsorption/activation, this is a likely explanation for the decrease in the charge transferred during the electrochemical-stripping phase. However, the source of the decrease in charge transfer for electrochemical stripping at electrode potential holds greater than 0.4 V vs RHE is less clear. We hypothesize that it is likely due either to the adsorption of hydroxide species competing with methane activation for Pt sites or a decrease in steady-state coverage of CO* because of more favorable oxidation kinetics. To test these hypotheses, we compared the total charge transferred during the electrode potential hold and stripping phase at two different electrode hold potentials.

Figure 5 shows the ratio of charge transferred during the electrode potential hold to the subsequent charge transferred during stripping, with each ratio plotted as a function of electrode potential hold length at 0.4 and 0.6 V vs RHE (see SI sections 7 and 8, Figures S9−S18 for CA and CV data). For electrode potential holds at 0.4 V vs RHE the charge ratio ($Q_{CA}/Q_{Stripping}$) is relatively constant at a value of ~3 for holds up to an hour in length. Notably, when we assume that the oxidation feature observed in the electrochemical-stripping phase is due to the $2e^-$ oxidation of adsorbed CO* to CO_2, as is supported by our DFT-derived free energy diagram (Figure 3), a ratio of ~3 suggests minimal CO oxidation during the electrode potential hold over the first hour. For time scales

DOI: 10.1021/acscatal.9b01207
ACS Catal. 2019, 9, 7578−7587

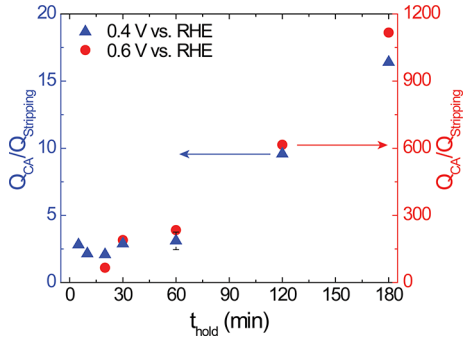

Figure 5. Ratio of charge transferred during the electrode potential hold (Q_{CA}) to the stripping feature ($Q_{Stripping}$) at an electrode hold potential of 0.4 V vs RHE (blue, left axis) and 0.6 V vs RHE (red, right axis) as a function of electrode potential hold length. Slopes were fit to the last three data points for each potential. No distinguishable stripping feature was observed at 5 and 10 min electrode potential holds at 0.6 V vs RHE.

greater than ~1 h, $Q_{CA}/Q_{Stripping}$ increases linearly with a slope of ~0.1 min^{-1} presumably because of steady-state oxidation of CO* on the surface.

The behavior of $Q_{CA}/Q_{Stripping}$ as a function of time is significantly different for electrode potential holds at 0.6 V vs RHE. First, the initial value of the charge ratio is ~30× larger than that for 0.4 V vs RHE. Second, although a linear increase in $Q_{CA}/Q_{Stripping}$ is also observed for the hold potential of 0.6 V vs RHE for hold times above 1 h, the slope is now 70× steeper (~7 min^{-1} at 0.6 V vs RHE vs ~0.1 min^{-1} 0.4 V vs RHE), suggesting an improvement in the overall reaction kinetics with increased potential. On the basis of these findings, we conclude that the smaller oxidation features observed after an electrode potential hold at 0.6 V vs RHE compared to 0.4 V vs RHE are the result of faster methane oxidation occurring at the increased holding potential, as opposed to the onset of OH* poisoning (which would decrease the number of available active sites and lower the rates). We will revisit this hypothesis in the context of our kinetic model.

3.4. Kinetic Modeling. In the following section, we develop a simple kinetic model for the electrochemical oxidation of methane on platinum. We consider the steps outlined below, in which eq 3 is rate-determining and all other steps are assumed to be equilibrated. Further details can be found in SI section 9.

$$CH_4 + 2* \xrightarrow{RDS} CH_3^* + H^* \quad (3)$$

$$CH_3^* + H_2O \leftrightarrow CO^* + 5H^+/e^- \quad (4)$$

$$H^* \leftrightarrow * + H^+/e^- \quad (5)$$

$$H_2O + * \leftrightarrow OH^* + H^+/e^- \quad (6)$$

$$OH^* + CO^* \leftrightarrow CO_2 + 2* + H^+/e^- \quad (7)$$

The assumption that methane activation is rate-limiting is common in the published literature[2,47−50] and implies that the kinetics of reactions between other methane-derived surface intermediates are relatively facile. We ignore other surface-bound methane derivatives between CH_3^* and CO*, because our calculations have shown CO* to be the most stable methane-derived surface intermediate. Given these assumptions, there are five energetic quantities relevant to our analysis: the binding energies of OH*, CO*, CH_3^*, and H* and the activation energy of CH_4. We note that CH_3^* and H* do not bind strongly enough to enter into the kinetics over the range of potentials considered as can be inferred from the free energy diagram presented in Figure 3. This is not the case for OH* and CO*; therefore, we compare our DFT estimates for these binding energies in addition to the CH_4 activation barrier to known experimental values to obtain more confidence in our results.

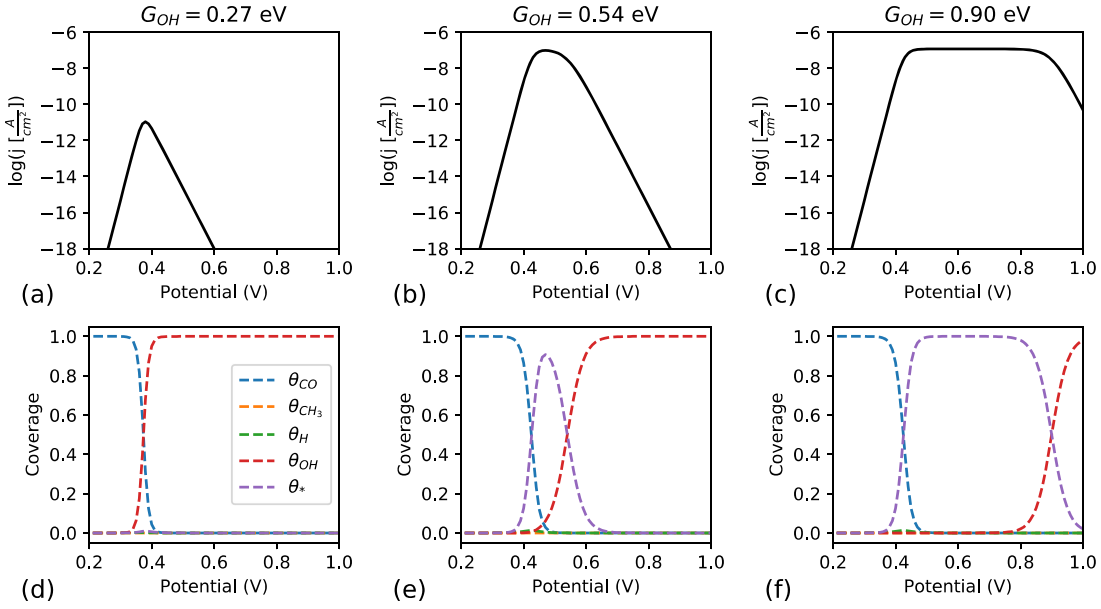

Figure 6. Methane oxidation kinetics for different values of OH* binding with P_{CH_4} = 1 bar and P_{CO_2} = 1 mbar. Panels (a−c) contain log current densities for G_{OH} = 0.27, 0.54, and 0.9 eV, respectively, as a function of electrochemical potential (V vs RHE) assuming a site density of 10^{15} sites/cm^2 and ~6.2% of the ECSA being active for methane oxidation (as in SI section 10); panels (d−f) contain coverages of key intermediates as a function of potential (V vs RHE) for G_{OH} = 0.27, 0.54, and 0.9 eV, respectively.

DOI: 10.1021/acscatal.9b01207
ACS Catal. 2019, 9, 7578−7587

The experimental integral CO* binding enthalpy at 50% coverage has previously been reported to be −1.76 eV,[51] which is equivalent to a CO* binding enthalpy relative to gaseous methane and water of 0.38 eV. This is in excellent agreement with our calculated integral binding enthalpy at 33% coverage of 0.43 eV. Using the harmonic adsorbate approximation, we calculate the Gibbs free energy of CO* binding relative to methane gas and liquid water at 300 K to be 0.30 eV.

As a result of the computational and methodological challenges that are characteristic of electrochemical barrier calculations,[52] we elect here to calculate only the thermochemical barrier for methane activation on Pt(211) in vacuum. Furthermore, we believe the consideration of only the thermochemical barrier is justified given that we observe relatively weak potential dependence for what is presumed to be the rate constant for methane activation observed experimentally (SI section 10, Figure S20). The thermochemical free energy barrier calculated for methane activation using harmonic transition-state theory (0.93 eV) is in excellent agreement with the effective barrier extracted from fitting the experimental data in this work (0.94−0.98 eV, SI section 10, Figure S21). Our calculated barrier also agrees favorably with sticking coefficients found for thermochemical methane activation on Pt(211).[37]

Finally, we calculate the equilibrium potential of OH* binding to be 0.54 eV after applying a small (−0.05 eV) solvation correction reported previously for Pt(533) steps.[39] However, we acknowledge that the equilibrium potential for OH* adsorption at Pt(100)-type steps is generally not agreed upon, arguably taking on values in acidic conditions as low as 0.27 V[40] or as high as 0.9 V, where anodic features are typically observed.[53] Therefore, we solve three kinetic models, each with a different representative OH* binding energy, and explore the resulting solutions. The current densities and surface coverages (denoted θ^i for surface species i) produced by these three kinetic models are shown in Figure 6.

In panels (b) and (e), we have assumed our DFT-calculated OH* binding equilibrium potential of 0.54 eV. We see in panel (e) that the CO* coverage is ∼1 at electrochemical potentials below ∼0.4 V; correspondingly, the rates of methane oxidation (shown in panel (b)) are quite small in this potential range because of active site poisoning. At sufficiently low potentials (not shown here), hydrogen will bind more favorably than CO*. As the electrochemical potential approaches 0.45 V, the point at which CO* → CO_2(g) equilibrium becomes thermodynamically downhill, the CO* coverage drops below ∼1, and CH_4 begins to continuously oxidize to CO_2 at rates on the order of 10 nA/cm^2, limited only by the thermal methane activation barrier (0.93 eV). Increasing the electrochemical potential further, OH* species begin to poison the surface (having an equilibrium binding potential of 0.54 V), and the rate drops again. Notably, the drop-off in CO* coverage centered around 0.45 V agrees with the decrease in the CO-stripping feature as a function of holding potential previously discussed in Figure 4b. Additionally, the increase in steady-state current from 0.4 to 0.6 V vs RHE observed experimentally (SI section 7, Figures S9 and S10) agrees favorably with our model, which shows that CO* poisoning is mitigated at higher electrochemical potentials because of the thermodynamics favoring CO_2 (step 5 becomes downhill) at these higher potentials. Although the sigmoid describing the CO* coverage has a width of only ∼0.1 V in this model, approximately half the width of the drop in the oxidation feature seen experimentally (Figure 4a), this difference could be explained by the repulsive CO*−CO* interactions known to exist on Pt(211) that are not considered in our model.[51]

We note here that our conclusion, namely, that methane oxidation is occurring continuously at an electrode potential of 0.6 V vs RHE, does not contradict the conclusions of the CO* monolayer oxidation literature, which find that the CO* oxidation feature occurs at higher potentials (e.g., between 0.7 and 0.85 V vs RHE).[42,54,55] Indeed, the oxidation feature during the electrochemical experiments conducted herein occurs at 0.8 V vs RHE, suggesting that our experimental setup is similar to those reported previously. The small rates of continuous methane oxidation (on the order of ∼10 nA/cm^2) that we measure at 0.6 V vs RHE are much lower than the rates needed to observe an oxidation feature at typical CV sweep rates.

To quantify the sensitivity of the model to less favorable OH* binding, we re-examine our analysis assuming an equilibrium potential for OH* binding of 0.9 V vs RHE (Figure 6c,f). Having assumed that methane activation is rate-determining, the only effect of increasing the OH* equilibrium potential is to fend off OH* poisoning until higher potentials, shifting the right leg of the volcano-shaped rate profile to higher potentials.

Finally, we assume a more negative equilibrium potential for OH* binding on platinum (0.27 V), as has been recently suggested.[40] The results of this analysis are shown in Figure 6a,d. It can be seen that the maximum rates are now smaller (10^{-11} A/cm^2) because of the more strongly bound OH* species poisoning the surface at low electrode hold potentials. The methane oxidation current predicted by this model at 0.6 V vs RHE (10^{-18} A/cm^2) is 11 orders of magnitude smaller than the experimentally observed current at 0.6 V vs RHE (0.08 μA/cm^2, SI section 7, Figure S10). This model considering OH* binding at 0.27 V also seems to contradict the observations that the CO*-stripping feature does not occur until 0.8 V vs RHE in our electrochemical experiments and 0.7 to 0.85 V vs RHE in previous monolayer CO oxidation experiments,[42,54,55] because OH* would be readily accessible at potentials as low as 0.4 V. To resolve these disparities, we would have to conclude that such a strongly bound OH* species is neither a poison nor an oxidant and has little effect on the surface chemistry.

To conclude, our simplified kinetic model consisting of rate-determining methane activation followed by OH* adsorption and CO−OH coupling reproduces many of the observed experimental results, such as the increase in steady-state current and decrease in CO* coverage as the electrode hold potential is increased from 0.4 to 0.6 V vs RHE. Additionally, our modeling suggests that the strongly bound OH* species that has been recently hypothesized is, if present, not acting as a significant poison of surface active sites nor as an oxidant.

4. OUTLOOK—EXTENSION TO OTHER CATALYSTS

To extend our kinetic model for electrochemical methane activation to other stepped metal surfaces, we note that the overall rate of methane oxidation in our model depends on the electrode potential, the CH_3^*, H*, CO*, and OH* binding free energies, and the methane activation free energy. We can reduce the dimensionality by observing that the CH_3^* and H* binding energies and methane activation energy scale linearly with the CO* binding energy (SI section 11, Figure S23). Additionally, we propose that the quantities of interest in

DOI: 10.1021/acscatal.9b01207
ACS Catal. 2019, 9, 7578−7587

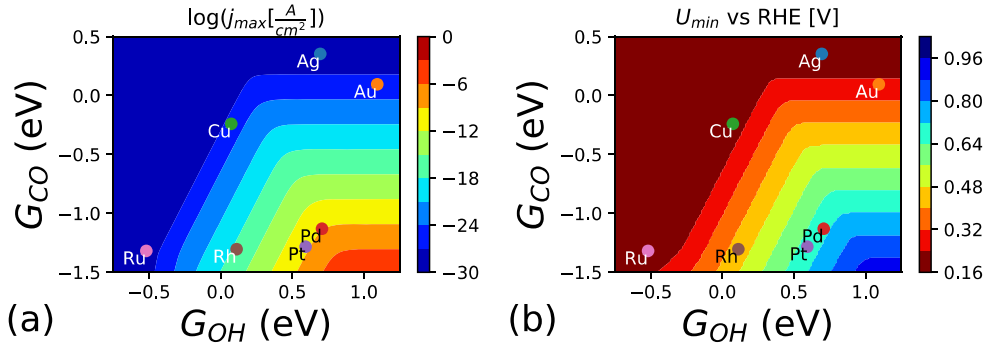

Figure 7. Contour plots for methane oxidation activity as a function of the free energy of adsorption of CO (relative to CO(g)) and OH (relative to $H_2O(l)/H_2(g)$). (a) The maximum attainable current density for electrochemical methane oxidation at ambient conditions for several metals and (b) the minimum electrochemical potential (V vs RHE) required to achieve the maximum current density.

continuous electrochemical methane oxidation are the maximum possible rate and the lowest electrode potential at which that rate can be achieved. Therefore, in Figure 7a, we show the maximum rate that can be achieved given the CO* and OH* binding energies of a catalyst, and in Figure 7b, we show the corresponding potential that needs to be applied to achieve that maximum rate.

We see that catalysts with strong CO* binding and weak OH* binding energies are desirable for high rates of methane oxidation but that we have to apply higher electrochemical potentials to achieve these increased rates. This can be understood as follows. To increase the rate of methane activation, we should decrease the methane activation barrier. Doing so increases the strength of CO* binding because of the linear scaling that exists between these two quantities. The surface will then be poisoned by CO*, unable to continuously oxidize methane at high rates, up to the electrode potential at which the CO* to CO_2 oxidation becomes thermodynamically favorable. Notably, this picture may indicate why Pt has been the most active transition metal catalyst to date for ambient temperature electrochemical methane oxidation. Pt has both one of the weakest OH* binding energies and one of the strongest CO* binding energies, leading to high rates of methane oxidation relative to the other transition metals.

To find a catalyst able to oxidize methane at significant rates and low electrochemical potentials, this model suggests we look to materials that diverge from the scaling between CO* and methane activation such that they bind CO* weakly but activate methane at significant rates. They should also possess weak OH* binding, which should not be problematic, because OH* binding is often not correlated with CO* binding.[56] Although traditional transition metal surfaces may not fulfill these requirements, other types of materials such as oxides, nitrides, alloys, or 2D materials might, and recent computational work suggests that metal oxides and MXenes ($AB_2C_2O_2$) catalysts have the potential to be selective toward methanol production from methane.[57]

Although our model successfully captures the activity of Pt and its strong performance compared to other metals, it is likely not a complete model for new materials screening. At sufficiently positive electrochemical potentials, it is likely that methane will be activated via an electrochemical pathway. Briefly, we note that considering methane activation via surface-bound O* or OH* or radical thermochemical routes would likely not lead to significant rates of methane oxidation on any of the transition metals considered based on previously published results.[58,59] However, an alternative pathway for methane activation involving a charged/electrochemical transition state via an O*/OH* promoter might allow weak-binding catalysts to become active at high potentials. We caution that this model will likely fail to describe catalyst performance at increased electrochemical potentials, but we also note that catalysts requiring significantly high electrode hold potentials may be of little practical interest. On a final note, when considering materials that activate methane at significant rates or bind OH* weakly, our assumption of methane activation being rate-determining may no longer be valid. In this case, considering the kinetics of CO−OH coupling would be necessary as we have done in SI Section 9.

In addition to considering materials besides Pt, another potential strategy indicated by our findings would be to increase temperature to facilitate faster methane oxidation rates. At 80 °C, a common temperature for fuel cell operation, we predict a 50-fold increase in the rate of methane activation, based on our electronic energy and entropy calculations (details in SI Section 11).

5. CONCLUSIONS

Through a combination of experimental results and DFT, we have developed new insight into the electrochemical oxidation of methane on platinum catalysts. Electrochemical experiments were used to probe methane activation and oxidation activity as a function of electrode potential and time. On the basis of our DFT calculations and comparison to the CO* monolayer oxidation literature, we concluded that the stable methane-derived surface intermediate was CO*. The optimum electrode potential for building up a coverage of CO* intermediate species on the platinum surface prior to electrochemical stripping was found to be 0.4 V vs RHE. Below this electrode hold potential, we hypothesized that methane activation was hindered by competition for active sites with strongly bound protons in the H_{UPD} region. However, at higher electrode hold potentials, particularly at 0.6 V vs RHE, we attribute the lower coverages of CO* to faster CO* oxidation kinetics. Our understanding of electrochemical methane oxidation on stepped Pt(211) was further probed via kinetic modeling. The sensitivity of our kinetic model to OH* binding energy was probed, and OH* equilibrium potentials of 0.54 and 0.9 V vs RHE were consistent with our experimental observations. The results of this kinetic model were extended to other stepped metal surfaces via a descriptor-based approach. Notably, platinum was predicted to be the most active (highest rate for methane activation) of all metals considered.

DOI: 10.1021/acscatal.9b01207
ACS Catal. 2019, 9, 7578−7587

Significant materials discovery efforts, including identifying catalysts that diverge from scaling between CO* binding energy and methane activation as outlined above, and/or alternative reaction schemes are needed to develop more active electrochemical catalysts for complete and partial oxidation of methane.

■ ASSOCIATED CONTENT

Supporting Information

The Supporting Information is available free of charge on the ACS Publications website at DOI: 10.1021/acscatal.9b01207.

Experimental details and additional data (PDF)

Folder of trajectory files used in DFT calculations (ZIP)

■ AUTHOR INFORMATION

Corresponding Authors

*E-mail: dhiggins@mcmaster.ca. (D.C.H.)
*E-mail: jaramillo@stanford.edu. (T.F.J.)
*E-mail: jkno@dtu.dk. (J.K.N.)

ORCID

Allegra A. Latimer: 0000-0003-3048-6593
Colin F. Dickens: 0000-0002-6151-0755
Adam C. Nielander: 0000-0002-3639-2427
Christopher Hahn: 0000-0002-2772-6341
Drew C. Higgins: 0000-0002-0585-2670
Thomas F. Jaramillo: 0000-0001-9900-0622

Notes

The authors declare no competing financial interest.

■ ACKNOWLEDGMENTS

We acknowledge support from the Natural Gas Initiative (NGI) at Stanford. This work was also supported by the U.S. Department of Energy, Chemical Sciences, Geosciences, and Biosciences (CSGB) Division of the Office of Basic Energy Sciences, via Grant DE-AC02-76SF00515 to the SUNCAT Center for Interface Science and Catalysis. Part of this work was performed at the Stanford Nano Shared Facilities (SNSF), supported by the National Science Foundation under award ECCS-1542152.

■ REFERENCES

(1) U.S. Energy Information Administration. Natural Gas Gross Withdrawals and Production. https://www.eia.gov/dnav/ng/ng_prod_sum_a_EPG0_VGV_mmcf_a.htm.

(2) Labinger, J. A. Selective alkane oxidation: hot and cold approaches to a hot problem. *J. Mol. Catal. A: Chem.* **2004**, *220* (1), 27−35.

(3) Periana, R. A.; Taube, D. J.; Gamble, S.; Taube, H.; Satoh, T.; Fujii, H. Platinum Catalysts for the High-Yield Oxidation of Methane to a Methanol Derivative. *Science* **1998**, *280* (5363), 560−564.

(4) O'Reilly, M. E.; Kim, R. S.; Oh, S.; Surendranath, Y. Catalytic Methane Monofunctionalization by an Electrogenerated High-Valent Pd Intermediate. *ACS Cent. Sci.* **2017**, *3* (11), 1174−1179.

(5) Horn, R.; Schlögl, R. Methane Activation by Heterogeneous Catalysis. *Catal. Lett.* **2015**, *145* (1), 23−39.

(6) Durante, V. A.; Walker, D. W.; Gussow, S. M.; Lyons, J. E. Silicometallate molecular sieves and their use as catalysts in oxidation of alkanes. EP0393895B1, 1990.

(7) Parfenov, M. V.; Starokon, E. V.; Pirutko, L. V.; Panov, G. I. Quasicatalytic and catalytic oxidation of methane to methanol by nitrous oxide over FeZSM-5 zeolite. *J. Catal.* **2014**, *318*, 14−21.

(8) Ipek, B.; Lobo, R. Catalytic conversion of methane to methanol on Cu-SSZ-13 using N 2 O as oxidant. *Chem. Commun.* **2016**, *52* (91), 13401−13404.

(9) Narsimhan, K.; Iyoki, K.; Dinh, K.; Román-Leshkov, Y. Catalytic Oxidation of Methane into Methanol over Copper-Exchanged Zeolites with Oxygen at Low Temperature. *ACS Cent. Sci.* **2016**, *2* (6), 424−429.

(10) Groothaert, M. H.; Smeets, P. J.; Sels, B. F.; Jacobs, P. A.; Schoonheydt, R. A. Selective Oxidation of Methane by the Bis(μ-oxo)dicopper Core Stabilized on ZSM-5 and Mordenite Zeolites. *J. Am. Chem. Soc.* **2005**, *127* (5), 1394−1395.

(11) Woertink, J. S.; Smeets, P. J.; Groothaert, M. H.; Vance, M. A.; Sels, B. F.; Schoonheydt, R. A.; Solomon, E. I. A $[Cu_2O]^{2+}$ core in Cu-ZSM-5, the active site in the oxidation of methane to methanol. *Proc. Natl. Acad. Sci. U. S. A.* **2009**, *106* (45), 18908−18913.

(12) Grundner, S.; Markovits, M. A. C.; Li, G.; Tromp, M.; Pidko, E. A.; Hensen, E. J. M.; Jentys, A.; Sanchez-Sanchez, M.; Lercher, J. A. Single-site trinuclear copper oxygen clusters in mordenite for selective conversion of methane to methanol. *Nat. Commun.* **2015**, *6*, 7546.

(13) Latimer, A. A.; Kakekhani, A.; Kulkarni, A. R.; Nørskov, J. K. Direct Methane to Methanol: The Selectivity−Conversion Limit and Design Strategies. *ACS Catal.* **2018**, *8* (8), 6894−6907.

(14) Bloomenergy. Bloomenergy Home Page. www.bloomenergy.com.

(15) Stoukides, M. Electrochemical studies of methane activation. *J. Appl. Electrochem.* **1995**, *25* (10), 899−912.

(16) Niedrach, L. W. The Performance of Hydrocarbons in Ion Exchange Membrane Fuel Cells. *J. Electrochem. Soc.* **1962**, *109* (11), 1092−1096.

(17) Perry, M. L.; Fuller, T. F. A Historical Perspective of Fuel Cell Technology in the 20th Century. *J. Electrochem. Soc.* **2002**, *149* (7), S59−S67.

(18) Niedrach, L. W. Studies of Hydrocarbon Fuel Cell Anodes by the Multipulse Potentiodynamic Method: II. Behavior of Methane on Conducting Porous Teflon Electrodes. *J. Electrochem. Soc.* **1966**, *113* (7), 645−650.

(19) Niedrach, L. W.; Tochner, M. Studies of Hydrocarbon Fuel Cell Anodes by the Multipulse Potentiodynamic Method: III. Behavior of Saturated Hydrocarbons on Conducting Porous Teflon Electrodes with a Phosphoric Acid Electrolyte. *J. Electrochem. Soc.* **1967**, *114* (1), 17−22.

(20) Taylor, A. H.; Brummer, S. B. The adsorption and oxidation of hydrocarbons on noble metal electrodes. VII. Oxidative adsorption of methane on platinum electrodes. *J. Phys. Chem.* **1968**, *72* (8), 2856−2862.

(21) Taylor, A. H.; Brummer, S. B. Adsorption and oxidation of hydrocarbons on noble metal electrodes. VIII. Composition of adsorbed methane and rate-limiting step in the overall methane to carbon dioxide reaction. *J. Phys. Chem.* **1969**, *73* (7), 2397−2403.

(22) Hsieh, S. Y.; Chen, K. M. Anodic Oxidation of Methane. *J. Electrochem. Soc.* **1977**, *124* (8), 1171−1174.

(23) Sustersic, M. G.; Córdova, O. R.; Triaca, W. E.; Arvía, A. J. The Electrosorption of Methane and Its Potentiodynamic Electrooxidation on Platinized Platinum. *J. Electrochem. Soc.* **1980**, *127* (6), 1242−1248.

(24) Hahn, F.; Melendres, C. A. Anodic oxidation of methane at noble metal electrodes: an 'in situ' surface enhanced infrared spectroelectrochemical study. *Electrochim. Acta* **2001**, *46* (23), 3525−3534.

(25) Kuhl, K. P.; Cave, E. R.; Abram, D. N.; Jaramillo, T. F. New insights into the electrochemical reduction of carbon dioxide on metallic copper surfaces. *Energy Environ. Sci.* **2012**, *5* (5), 7050−7059.

(26) Giannozzi, P.; Baroni, S.; Bonini, N.; Calandra, M.; Car, R.; Cavazzoni, C.; Ceresoli, D.; Chiarotti, G. L.; Cococcioni, M.; Dabo, I.; Dal Corso, A.; de Gironcoli, S.; Fabris, S.; Fratesi, G.; Gebauer, R.; Gerstmann, U.; Gougoussis, C.; Kokalj, A.; Lazzeri, M.; Martin-Samos, L.; Marzari, N.; Mauri, F.; Mazzarello, R.; Paolini, S.; Pasquarello, A.; Paulatto, L.; Sbraccia, C.; Scandolo, S.; Sclauzero, G.; Seitsonen, A. P.; Smogunov, A.; Umari, P.; Wentzcovitch, R. M.

DOI: 10.1021/acscatal.9b01207
ACS Catal. 2019, 9, 7578−7587

QUANTUM ESPRESSO: a modular and open-source software project for quantum simulations of materials. *J. Phys.: Condens. Matter* **2009**, *21* (39), 395502.
(27) Hammer, B.; Hansen, L. B.; Nørskov, J. K. Improved adsorption energetics within density-functional theory using revised Perdew-Burke-Ernzerhof functionals. *Phys. Rev. B: Condens. Matter Mater. Phys.* **1999**, *59* (11), 7413−7421.
(28) Hohenberg, P.; Kohn, W. Inhomogeneous Electron Gas. *Phys. Rev.* **1964**, *136* (3B), B864−B871.
(29) Kohn, W.; Sham, L. J. Self-Consistent Equations Including Exchange and Correlation Effects. *Phys. Rev.* **1965**, *140* (4A), A1133−A1138.
(30) Henkelman, G.; Uberuaga, B. P.; Jónsson, H. A climbing image nudged elastic band method for finding saddle points and minimum energy paths. *J. Chem. Phys.* **2000**, *113* (22), 9901−9904.
(31) Henkelman, G.; Jónsson, H. Improved tangent estimate in the nudged elastic band method for finding minimum energy paths and saddle points. *J. Chem. Phys.* **2000**, *113* (22), 9978−9985.
(32) Garrity, K. F.; Bennett, J. W.; Rabe, K. M.; Vanderbilt, D. Pseudopotentials for high-throughput DFT calculations. *Comput. Mater. Sci.* **2014**, *81*, 446−452.
(33) Hjorth Larsen, A.; Jørgen Mortensen, J.; Blomqvist, J.; Castelli, I. E.; Christensen, R.; Dułak, M.; Friis, J.; Groves, M. N.; Hammer, B.; Hargus, C.; Hermes, E. D.; Jennings, P. C.; Bjerre Jensen, P.; Kermode, J.; Kitchin, J. R.; Leonhard Kolsbjerg, E.; Kubal, J.; Kaasbjerg, K.; Lysgaard, S.; Bergmann Maronsson, J.; Maxson, T.; Olsen, T.; Pastewka, L.; Peterson, A.; Rostgaard, C.; Schiøtz, J.; Schütt, O.; Strange, M.; Thygesen, K. S.; Vegge, T.; Vilhelmsen, L.; Walter, M.; Zeng, Z.; Jacobsen, K. W. The atomic simulation environment—a Python library for working with atoms. *J. Phys.: Condens. Matter* **2017**, *29* (27), 273002.
(34) Peterson, A. A.; Abild-Pedersen, F.; Studt, F.; Rossmeisl, J.; Nørskov, J. K. How copper catalyzes the electroreduction of carbon dioxide into hydrocarbon fuels. *Energy Environ. Sci.* **2010**, *3* (9), 1311−1315.
(35) Blaylock, D. W.; Ogura, T.; Green, W. H.; Beran, G. J. O. Computational Investigation of Thermochemistry and Kinetics of Steam Methane Reforming on Ni(111) under Realistic Conditions. *J. Phys. Chem. C* **2009**, *113* (12), 4898−4908.
(36) Jiang, T.; Mowbray, D. J.; Dobrin, S.; Falsig, H.; Hvolbæk, B.; Bligaard, T.; Nørskov, J. K. Trends in CO Oxidation Rates for Metal Nanoparticles and Close-Packed, Stepped, and Kinked Surfaces. *J. Phys. Chem. C* **2009**, *113* (24), 10548−10553.
(37) Chadwick, H.; Guo, H.; Gutiérrez-González, A.; Menzel, J. P.; Jackson, B.; Beck, R. D. Methane dissociation on the steps and terraces of Pt(211) resolved by quantum state and impact site. *J. Chem. Phys.* **2018**, *148* (1), No. 014701.
(38) McCrum, I. T.; Janik, M. J. pH and Alkali Cation Effects on the Pt Cyclic Voltammogram Explained Using Density Functional Theory. *J. Phys. Chem. C* **2016**, *120* (1), 457−471.
(39) McCrum, I. T.; Janik, M. J. First Principles Simulations of Cyclic Voltammograms on Stepped Pt(553) and Pt(533) Electrode Surfaces. *ChemElectroChem* **2016**, *3* (10), 1609−1617.
(40) van der Niet, M. J. T. C.; Garcia-Araez, N.; Hernández, J.; Feliu, J. M.; Koper, M. T. M. Water dissociation on well-defined platinum surfaces: The electrochemical perspective. *Catal. Today* **2013**, *202*, 105−113.
(41) Lebedeva, N. P.; Rodes, A.; Feliu, J. M.; Koper, M. T. M.; van Santen, R. A. Role of Crystalline Defects in Electrocatalysis: CO Adsorption and Oxidation on Stepped Platinum Electrodes As Studied by in situ Infrared Spectroscopy. *J. Phys. Chem. B* **2002**, *106* (38), 9863−9872.
(42) Arenz, M.; Mayrhofer, K. J. J.; Stamenkovic, V.; Blizanac, B. B.; Tomoyuki, T.; Ross, P. N.; Markovic, N. M. The Effect of the Particle Size on the Kinetics of CO Electrooxidation on High Surface Area Pt Catalysts. *J. Am. Chem. Soc.* **2005**, *127* (18), 6819−6829.
(43) Bjerke, A. E.; Griffiths, P. R.; Theiss, W. Surface-Enhanced Infrared Absorption of CO on Platinized Platinum. *Anal. Chem.* **1999**, *71* (10), 1967−1974.
(44) Marković, N. M.; Lucas, C. A.; Rodes, A.; Stamenković, V.; Ross, P. N. Surface electrochemistry of CO on Pt(111): anion effects. *Surf. Sci.* **2002**, *499* (2), L149−L158.
(45) Tang, W.; Peterson, A. A.; Varela, A. S.; Jovanov, Z. P.; Bech, L.; Durand, W. J.; Dahl, S.; Nørskov, J. K.; Chorkendorff, I. The importance of surface morphology in controlling the selectivity of polycrystalline copper for CO2 electroreduction. *Phys. Chem. Chem. Phys.* **2012**, *14* (1), 76−81.
(46) Nørskov, J. K.; Studt, F.; Abild-Pedersen, F.; Bligaard, T. *Fundamental concepts in heterogeneous catalysis*; John Wiley & Sons, 2014.
(47) Cant, N. W.; Lukey, C. A.; Nelson, P. F.; Tyler, R. J. The rate controlling step in the oxidative coupling of methane over a lithium-promoted magnesium oxide catalyst. *J. Chem. Soc., Chem. Commun.* **1988**, *12*, 766−768.
(48) Li, W.; He, D.; Hu, G.; Li, X.; Banerjee, G.; Li, J.; Lee, S. H.; Dong, Q.; Gao, T.; Brudvig, G. W.; Waegele, M. M.; Jiang, D.-e.; Wang, D. Selective CO Production by Photoelectrochemical Methane Oxidation on TiO2. *ACS Cent. Sci.* **2018**, *4* (5), 631−637.
(49) German, E. D.; Sheintuch, M. Predicting CH4 Dissociation Kinetics on Metals: Trends, Sticking Coefficients, H Tunneling, and Kinetic Isotope Effect. *J. Phys. Chem. C* **2013**, *117* (44), 22811−22826.
(50) Kumar, G.; Lau, S. L. J.; Krcha, M. D.; Janik, M. J. Correlation of Methane Activation and Oxide Catalyst Reducibility and Its Implications for Oxidative Coupling. *ACS Catal.* **2016**, *6* (3), 1812−1821.
(51) Karmazyn, A. D.; Fiorin, V.; Jenkins, S. J.; King, D. A. First-principles theory and microcalorimetry of CO adsorption on the {211} surfaces of Pt and Ni. *Surf. Sci.* **2003**, *538* (3), 171−183.
(52) Rossmeisl, J.; Skúlason, E.; Björketun, M. E.; Tripkovic, V.; Nørskov, J. K. Modeling the electrified solid−liquid interface. *Chem. Phys. Lett.* **2008**, *466* (1), 68−71.
(53) Clavilier, J.; Armand, D.; Sun, S. G.; Petit, M. Electrochemical adsorption behaviour of platinum stepped surfaces in sulphuric acid solutions. *J. Electroanal. Chem. Interfacial Electrochem.* **1986**, *205* (1), 267−277.
(54) Lebedeva, N. P.; Koper, M. T. M.; Herrero, E.; Feliu, J. M.; van Santen, R. A. Cooxidation on stepped Pt[n(111)×(111)] electrodes. *J. Electroanal. Chem.* **2000**, *487* (1), 37−44.
(55) Calle-Vallejo, F.; Pohl, M. D.; Bandarenka, A. S. Quantitative Coordination−Activity Relations for the Design of Enhanced Pt Catalysts for CO Electro-oxidation. *ACS Catal.* **2017**, *7* (7), 4355−4359.
(56) Peterson, A. A.; Nørskov, J. K. Activity Descriptors for CO2 Electroreduction to Methane on Transition-Metal Catalysts. *J. Phys. Chem. Lett.* **2012**, *3* (2), 251−258.
(57) Arnarson, L.; Schmidt, P. S.; Pandey, M.; Bagger, A.; Thygesen, K. S.; Stephens, I. E. L.; Rossmeisl, J. Fundamental limitation of electrocatalytic methane conversion to methanol. *Phys. Chem. Chem. Phys.* **2018**, *20*, 11152.
(58) Yoo, J. S.; Khan, T. S.; Abild-Pedersen, F.; Nørskov, J. K.; Studt, F. On the role of the surface oxygen species during A−H (A = C, N, O) bond activation: a density functional theory study. *Chem. Commun.* **2015**, *51* (13), 2621−2624.
(59) Latimer, A. A.; Aljama, H.; Kakekhani, A.; Yoo, J. S.; Kulkarni, A.; Tsai, C.; Garcia-Melchor, M.; Abild-Pedersen, F.; Nørskov, J. K. Mechanistic insights into heterogeneous methane activation. *Phys. Chem. Chem. Phys.* **2017**, *19* (5), 3575−3581.

DOI: 10.1021/acscatal.9b01207
ACS Catal. 2019, 9, 7578−7587